Spectroscopic and Calorimetric Analyses of Invasion Plasmid Antigen D (IpaD) from *Shigella flexneri* Reveal the Presence of Two Structural Domains†

Marianela Espina,‡ S. Fernando Ausar,§ C. Russell Middaugh,§ William D. Picking,‡ and Wendy L. Picking*,‡

Departments of Molecular Biosciences and Pharmaceutical Chemistry, University of Kansas, Lawrence, Kansas 66045

Received March 29, 2006; Revised Manuscript Received June 8, 2006

ABSTRACT: *Shigella flexneri* is a facultative intracellular pathogen that causes severe gastroenteritis in humans. Invasion plasmid antigen D (IpaD) is an essential participant in *Shigella* invasion of intestinal cells, but no detailed structural information is available to help understand the proposed role of IpaD in invasion or its interaction with other invasion proteins. Therefore, the secondary and tertiary structure and thermal stability of IpaD as well as selected IpaD deletion mutants were investigated using Fourier transform infrared (FTIR), circular dichroism (CD), and both intrinsic and extrinsic fluorescence spectroscopies. The energetics of thermal unfolding were also evaluated by differential scanning calorimetry (DSC). Secondary-structure analysis by CD and FTIR suggests that that IpaD is primarily α-helical with characteristics of a intramolecular coiled coil. Thermal studies revealed that the unfolding of IpaD is a complex process consisting of two transitions centered near 59 and 80 °C. A comparison of the data obtained with the intact protein and selected deletion mutants indicated that the lower temperature transition is a reversible event attributable to the unfolding of a small domain located at the N terminus of IpaD. In contrast, the thermal unfolding of the proposed major and highly stable C-terminal domain was irreversible and led to protein aggregation. When the results are taken together, they strongly support the idea that IpaD has two independent folding domains.

Shigella flexneri, like several others Gram-negative bacteria, use a type-III secretion system (TTSS)[1] to translocate effector proteins across the bacterial double membrane and into the cytoplasm of target eukaryotic cells (*1*). The structural proteins that form this "molecular syringe and needle", as well as the secreted effector proteins, are encoded in a 31-kb fragment of a large virulence plasmid (*2*). Within this fragment, the *mxi*/*spa* operon encodes the type-III secretion apparatus and the *ipa*/*ipg* operon encodes the secreted effector proteins (*3*, *4*). Of the *Shigella* TTSS effectors, IpaB, IpaC, and invasion plasmid antigen D (IpaD) are absolutely necessary for host-cell invasion by this pathogen (*5*). Prior to its secretion, IpaD has been proposed to interact with IpaB to form a "plug" that prevents IpaB and IpaC secretion until the proper extracellular stimulus is received (*6*). The loss of either "plug" component causes massive secretion of the TTSS effectors (*6*). Upon physical contact with the host cell, the bacterium inserts IpaB and IpaC into the host membrane to form a 2.5 nm pore that allows other effectors to enter the cell (*7*). Additionally, IpaB and IpaC have effector functions promoting apoptosis in macrophages and actin rearrangement in epithelial cells, respectively (*8*−*10*). How IpaD functions to control secretion, however, is unknown.

Deletion mutagenesis spanning the entire protein has shown that IpaD is involved in more than just secretion control (*11*). As with other TTSS secreted proteins, the IpaD secretion signal lies within the first 20 residues. Thus, deletion of the first 20 amino acids of IpaD prevents its secretion and gives rise to an *ipaD* null-like phenotype (*12*, *13*). Downstream of the secretion signal, 40 residue deletions ($IpaD^{\Delta 41-80}$ and $IpaD^{\Delta 81-120}$) in the N-terminal third of IpaD do not greatly effect invasion but give rise to intermediate levels of uninduced secretion (*11*). A significant reduction in hemolysis, however, is seen for these mutants that is due to a decreased efficiency of IpaB−IpaC insertion into erythrocyte membranes (*11*). In contrast, 40 residue deletions across the remainder of IpaD completely eliminate the invasive phenotype and cause secretion of massive amounts of IpaB, IpaC, and IpaD (*11*). More recently, we have shown that IpaD is located at the TTSS needle tip, which is a prerequisite for virulence functions (Espina et al., *Infect. Immun.*, in press). N-Terminal deletion mutants that give rise to strains with invasive phenotypes have surface-localized IpaD, while the C-terminal mutants that result in noninvasive strains lack IpaD on their surface. Furthermore, antibodies that recognize the N-terminal domain can neutralize hemolysis, while antibodies to the C terminus do not (Espina et al., *Infect. Immun.*, in press). These data point to the possibility that IpaD has two functional domains, with one being at the N terminus and one at the C terminus.

† This work was supported by PHS Grants AI034428 and AI057927 to W.D.P.

* To whom correspondence should be addressed: Department of Molecular Biosciences, University of Kansas, 1200 Sunnyside Avenue, Lawrence, KS 66045. Telephone: (785) 864-3299. Fax: (785) 864-5294. E-mail: pickingw@ku.edu.

‡ Department of Molecular Biosciences.

§ Department of Pharmaceutical Chemistry.

[1] Abbreviations: IpaD, invasion plasmid antigen D; TTSS, type-III secretion system; FTIR, Fourier transform infrared; CD, circular dichroism; ANS, 8-anilino-1-naphthalene sulfonate; DSC, differential scanning calorimetry.

10.1021/bi060625v CCC: $33.50
Published on Web 07/11/2006

In *Yersinia* spp., a protein with significant sequence homology to IpaD has not been found. LcrV, however, does appear to be its functional homologue. Similar to IpaD, LcrV has recently been found at the tip of the TTSA needle (*14*). Additionally, the deletion of LcrV prevents proper insertion of the *Yersinia* translocators, YopB and YopD, into erythrocyte membranes (*15*, *16*), while antibodies against LcrV protect erythrocytes from lysis by *Yersinia* (*17*). The atomic structure of LcrV has been solved, demonstrating a dumbbell-shaped protein consisting of a long coiled coil with a domain at each end of the coil (*18*). Little, however, is known about the structure−function relationships of LcrV.

In this study, the structural properties of IpaD were examined using a battery of complementary biophysical methods. Purified recombinant IpaD and three N-terminal mutants were used to investigate the structure and conformational stability of IpaD to provide insight into the functional data. The unfolding of IpaD occurs as a two-step process, suggesting the presence of two structural domains. The thermally labile N-terminal domain is proposed to be responsible for translating extracellular secretion signals to the bacterium, while the thermally stable C-terminal domain contains a intramolecular coiled coil and is proposed to preserve the structural integrity of the protein while maintaining a position at the *Shigella* TTSS needle tip. The two domains work in concert to control the productive release and presentation of IpaB and IpaC to the host-cell membrane.

EXPERIMENTAL PROCEDURES

Preparation of Affinity-Purified Recombinant Proteins. The *ipaD* mutant genes were subcloned from pWPsf4 into pET15b by previously described methods (*12*). The resulting plasmids were transformed into *Escherichia coli* Tuner (DE3) (Novagen, Madison, WI) with the recombinant proteins purified as previously described (*19*), dialyzed against 10 mM Na_2HPO_4 (pH 7.0) and 150 mM NaCl [phosphate-buffered saline (PBS)] and stored at −70 °C. Protein concentrations were determined by measuring the absorbance at 280 nm using extinction coefficients based on the amino acid composition of each protein (*20*), which varied minimally (10%) with the experimentally determined extinction coefficient (*21*).

Far-UV Circular Dichroism (CD) Spectroscopy. Far-UV CD spectra were collected using a Jasco J720 spectropolarimeter equipped with a Peltier temperature controller (Jasco, Inc., Easton, MD). Spectra were acquired using a 0.1 cm path-length cuvette at 37 °C. A resolution of 0.5 nm and a scanning speed of 20 nm/min with a 2 s response time were employed. Spectra presented are an average of three consecutive measurements. Secondary-structure content was estimated using the Dichroweb software package (*22*, *23*), which allows for the analysis of secondary-structure content using the algorithms CONTIN (*24*), SELCON (*25*), and CDSSTR (*26*). The thermal unfolding of the proteins was followed by monitoring the ellipticity at 222 nm over a temperature range of 10−90 °C with a resolution of 0.5 °C and a 15 °C/h heating rate. A protein concentration of 0.1 mg/mL was employed in all measurements. CD signals were converted to mean residue molar ellipticities $[\theta]_R$, and the thermal transitions were analyzed using the Jasco Spectral Manager and Microcal Origin 6.0 software (*27*).

FTIR Spectroscopy. The secondary structure of IpaD and $IpaD^{\Delta 1-120}$ in solution was also assessed using Fourier transform infrared (FTIR) spectroscopy. Samples of 1 mL of protein in D_2O (15 mg/mL) were placed onto a ZnSe attenuated total reflectance (ATR) crystal (Spectra-Tech, Shelton, CT). The exchange into D_2O was done by lyophilization of the protein and resuspension in D_2O at a pD of 7.0. The pD value of the protein solution was measured with a standard pH-meter and corrected according to pD = pH + 0.4. Data were collected using 256 scans with a resolution of 4 cm^{-1} with an ABB Bomen FTIR MB series spectrometer (ABB, Bomen, Quebec, Canada). A thermal A.R.K. temperature controller (Spectra-Tech, Shelton, CT) was used to increase the temperature from 25 to 90 °C at 5 °C intervals. A spectrum at each temperature was obtained by equilibrating the sample for 3 min at each temperature prior to data collection. D_2O spectra were collected under identical conditions and subtracted from the spectra of the proteins at the corresponding temperature. The amide I′ region was fit with Gaussian band profiles using GRAMS/386 software (Galactic, Inc.). The number of bands and their position were taken from the second-derivative trace of the amide I′ band and the Fourier self-deconvolution (FSD) maxima. The FSD calculations were performed in OMNIC software (Nicolet Instrument, Madison, WI) using a bandwidth of 17 cm^{-1} and a band-narrowing factor of 2.0.

Intrinsic and Extrinsic Fluorescence Spectroscopy. Tryptophan fluorescence studies were performed by monitoring the intrinsic fluorescence using an excitation of 280 nm, an emission range of 300−450 nm, and a resolution of 1 nm. Steady-state fluorescence spectra were recorded using a PTI QuantaMaster spectrophotometer with a Peltier-controlled cuvette holder. The protein concentration used was 0.1 mg/mL. A 1 cm path-length cuvette with a Teflon cap was used in all experiments. Spectra were collected from 10 to 90 °C at 2.5 °C intervals with a 3 min equilibration time at each temperature. Tryptophan peak positions were determined by first-derivative analysis. Data analysis was performed using Felix (PTI) and Microcal Origin software.

To further investigate the stability of the IpaD and its mutants, samples (0.1 mg/mL) in the presence of 100 μM 8-anilino-1-naphthalene sulfonate (ANS) were excited at 385 nm and the emission spectrum of the dye was recorded from 400 to 580 nm as a function of the temperature. Excitation and emission slits were set at 2 and 4 nm, respectively, and a 5 min hold time was used at each temperature prior to data collection. Emission spectra of 100 μM ANS in buffer alone were subtracted from sample spectra at each temperature.

Temperature-Induced Protein Aggregation. The aggregation of the proteins as a function of the temperature was studied by monitoring the turbidity of the solution at 360 nm with a Hewlett−Packard 8453 UV−vis spectrophotometer (Agilent, Palo Alto, CA) equipped with a Peltier temperature controller. A protein concentration of 0.1 mg/mL was used for all experiments.

Differential Scanning Calorimetry (DSC). Calorimetric experiments were performed with a MicroCal VP-DSC high throughput capillary differential scanning calorimeter (Northampton, MA). DSC thermograms were obtained from 10 to 115 °C at a scan rate of 1 °C/min with a protein concentration of 2 mg/mL in PBS. Baseline correction was

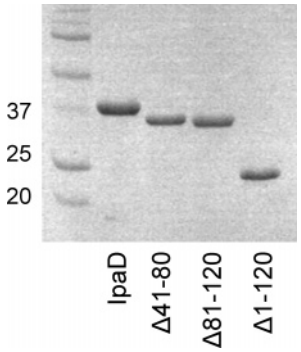

FIGURE 1: SDS−PAGE of purified recombinant proteins. IpaD, IpaD$^{\Delta 41-80}$, IpaD$^{\Delta 81-120}$, and IpaD$^{\Delta 1-120}$ were subjected to SDS−PAGE and then stained with Coomassie Blue R-250. Molecular weights are shown at the left.

performed by subtracting a buffer thermogram obtained under identical conditions. After the first scan, the samples were cooled and rescanned to check the reversibility of the unfolding process. The data were analyzed using MicroCal Origin 7.0 (Origin-Lab Corporation, Northampton, MA) assuming a non-two-state unfolding model (*28*).

RESULTS

Generation of IpaD and IpaD Deletion Mutants. Currently, biochemical knowledge regarding IpaD is limited to it being a monomeric 332 amino acid protein that is highly soluble with a pI of 5.5 (W. Picking, unpublished data and ref *19*). To provide further insight into the IpaD structure, a biophysical examination of IpaD and several N-terminal, internal, and C-terminal deletion mutants was initiated. Of the 40 residue deletion mutants that span IpaD, only two recombinant proteins, IpaD$^{\Delta 41-80}$ and IpaD$^{\Delta 81-120}$, could be purified from the bacterial cytoplasm (Figure 1). All other recombinant 40 residue deletion mutants were sequestered into bacterial inclusion bodies. When large deletions were made from the N terminus and the proteins were expressed in *E. coli*, recombinant IpaD$^{\Delta 1-120}$ remained soluble, while IpaD$^{\Delta 1-160}$ partitioned into inclusion bodies (Figure 1). Similarly, when deletions were introduced from the C terminus, only proteins having small deletions (i.e., IpaD$^{\Delta 321-332}$ and IpaD$^{\Delta 328-332}$) remained soluble, while larger deletions (i.e., IpaD$^{\Delta 241-332}$) were found in inclusion bodies. Because the large deletions introduced into the C-terminal portion of IpaD gave rise to proteins that were degraded and led to uncontrolled secretion in *S. flexneri*, these proteins were assumed to be unstable and/or misfolded and were not further analyzed (*11*). Although IpaD mutants possessing small deletions (5−12 residues) at the C terminus resulted in noninvasive phenotypes, which secreted large amounts of IpaB, IpaC, and IpaD (*11*), they showed biophysical properties and stability identical to that of IpaD. Because these deletions have no impact on the overall structure of IpaD, a correlation between altered structure and altered function cannot be made (Espina et al., *Infect. Immun.*, in press).

Secondary-Structure Analysis of IpaD by CD Spectroscopy. Initially, the secondary structure and thermostability of IpaD was analyzed using CD spectroscopy. The far-UV CD spectrum of IpaD displays double minima at 208 and 222 nm, suggesting a significant amount of helical structure (Figure 2A). The secondary-structure content was estimated

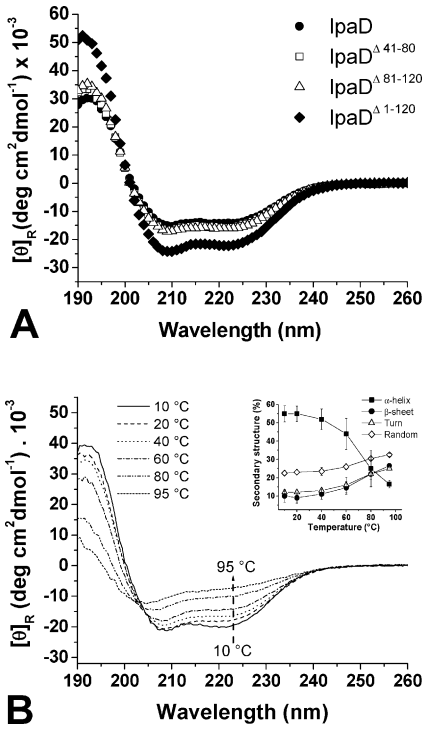

FIGURE 2: CD spectroscopy studies of IpaD and its N-terminal deletion mutants. (A) Far-UV CD spectra of IpaD and N-terminal deletion mutants were recorded at 37 °C in 10 mM phosphate buffer at pH 7.4. (B) Far-UV CD spectra of IpaD at pH 7.4 as a function of the temperature from 10 to 95 °C, and the secondary-structure contents were estimated from these spectra using CDSSTR (inset). All spectra presented are an average of three consecutive scans.

Table 1: Secondary-Structure Estimates for IpaD and IpaD Mutants[a]

protein	α helix	β sheet	turn	random
IpaD	50.0 ± 1.5[b]	11.0 ± 0.2	15.0 ± 0.3	24.0 ± 0.5
IpaD$^{\Delta 41-80}$	52.5 ± 0.7	10.0 ± 0.3	13.0 ± 0.4	24.0 ± 0.6
IpaD$^{\Delta 81-120}$	54.5 ± 0.7	9.0 ± 0.0	12.5 ± 0.7	23.0 ± 0.5
IpaD$^{\Delta 1-120}$	71.0 ± 1.0	4.5 ± 0.7	7.0 ± 0.0	17.0 ± 0.7

[a] The estimated percent content of each type of secondary structure is provided. [b] Standard error ($n = 3$).

from the far-UV CD spectra using the Dichroweb suite of algorithms (*22*, *23*), with CDSSTR (*26*) being chosen for the final secondary-structure analysis because it provided the best fit to the observed spectra. The results indicate that IpaD is predominantly an α-helical protein, with some β-sheet and disordered structure being present (Table 1). The three N-terminal mutants analyzed showed CD spectra similar to that of IpaD (Figure 2A). Although no major changes were observed in the distribution of the secondary structure among the IpaD N-terminal deletion mutants, all three such mutants displayed a relatively larger amount of helical structure than IpaD itself (Table 1). These results suggest that the N terminus of IpaD maybe relatively richer in nonhelical structures than the C-terminal region. For IpaD$^{\Delta 1-120}$, this result is consistent with the idea that each TTSS-secreted protein contains a 20 amino acid sequence at the N terminus that is predicted to be unstructured but is required for secretion through the apparatus (*13*).

To study the conformational changes occurring in IpaD secondary structure upon heating, the far-UV spectra were recorded as a function of the temperature and the distribution

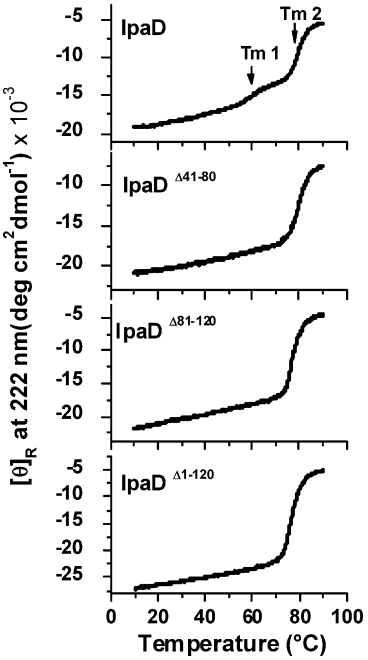

FIGURE 3: Temperature dependence of the molar ellipticity at 222 nm of IpaD and N-terminal mutants. Ellipticity at 222 nm was monitored from 10 to 90 °C at 0.5 °C intervals at a rate of 15 °C/h. Protein concentrations were 0.1 mg/mL. The positions of the minor (Tm1) and major (Tm2) thermal transitions are indicated by arrows for IpaD. Although the error bars have been omitted for clarity, the individual data entries have a typical uncertainty of less than 5% ($n = 3$).

of the secondary structure was calculated using CDSSTR (Figure 2B). As the temperature increased, a gradual loss of ellipticity is observed in the far-UV CD spectrum with a substantial decrease at 222 nm after reaching 40 °C when a notable decrease in the helical structure was observed with the appearance of a spectral shape characteristic of a mixture of disordered and β structures. The distribution of the secondary structure showed a progressive decrease in the α-helical component, concomitant with an increase in random coil, β sheet, and turns (inset of Figure 2B).

The comparative thermal stabilities of IpaD and the N-terminal mutants were determined by monitoring the changes in the ellipticity at 222 nm as a function of the temperature (Figure 3). IpaD displayed two apparent thermal transitions, one minor and one major, at about 60 and 80 °C, respectively, suggesting the presence of two separately folding domains (labeled as Tm1 and Tm2 in Figure 3). No reversibility was observed when the sample was cooled to 10 °C and reheated to 90 °C. In a separate experiment, the ellipticity at 222 nm and the spectra of IpaD were monitored up to the end of the minor transition (70 °C) and recooled to 10 °C. Under these conditions, the heating traces as well as the T_m obtained were indistinguishable from those observed initially (data not shown). These results provide strong evidence that the lower temperature transition event is thermally reversible. The three N-terminal mutants under study only displayed a single transition at about 80 °C, suggesting that the structural domain responsible for the low-temperature transition resides at the IpaD N terminus (Figure 3).

Secondary-Structure Analysis of IpaD and IpaD$^{\Delta 1-120}$ by FTIR. The secondary structure of IpaD and the N-terminal deletion mutant, IpaD$^{\Delta 1-120}$, was further analyzed by FTIR spectroscopy. The amide I′ region of IpaD at 25 °C dissolved in D_2O was decomposed into its component peaks based on Fourier self-deconvolution and the second-derivative trace (Figure 4A). The peak deconvolution showed three predominant bands at 1630.7, 1643.1, and 1653.5 cm^{-1}. Additional minor bands were also observed at higher and lower frequencies (Figure 4A). Using the classical assignments for FTIR spectra (*29*), it seems that IpaD is composed predominantly of β strand (peak ∼ 1630 cm^{-1}) and unordered structure (peak ∼ 1643.1 cm^{-1}), with less than 30% of the peak area found in the traditional α-helix position (peak ∼ 1653 cm^{-1}). These results strongly disagreed with the CD spectroscopy observations. Therefore, after sample preparation for FTIR measurements, the CD spectrum was again recorded to discard the unfolded protein induced by the concentration, lyophilization, and dissolution of the IpaD in D_2O. Under this circumstance, the CD spectrum of IpaD was found to be identical to that observed for the nontreated samples, showing the typical α-helix signature as reported in Figure 2A. The IR spectral deviation from the classical α helix can be interpreted as a distortion of the helical parameter because of the supercoil bending of helices arranged in coiled-coil structures. The triplet of equally strong bands observed in the FTIR spectrum (Figure 4A) of IpaD has been indicated as a spectral fingerprint of intramolecular coiled-coil proteins (*30*, *31*). In very good agreement, in silico analyses (*32*) predict that IpaD is largely α-helical with an internal coiled coil involving residues 130−174 and 270−315 (data not shown). The N-terminal deletion mutant IpaD$^{\Delta 1-120}$ displayed peak deconvolution profiles similar to its wild-type counterpart, indicating that the deletion did not significantly alter the coiled-coil region (data not shown). The thermal unfolding of IpaD was also studied by monitoring the changes induced in the amide I′ region of the spectra by the temperature (Figure 4B). As the temperature is increased, the amide I′ region became broader because of the emergence of two peaks at 1680 and 1616.5 cm^{-1}. Two such bands are characteristic of the formation of intermolecular β-sheet structure and have been extensively reported in irreversibly aggregated proteins (*33*, *34*). The temperature-dependent changes in the peak area at 1616.5 cm^{-1} showed a single temperature transition at around 75 °C, which agrees with the high-temperature transition (Tm2) observed by CD. A similar behavior with respect to the temperature of this peak was observed for the IpaD$^{\Delta 1-120}$ mutant (Figure 4C). These results indicate that the thermal unfolding of the major C-terminal domain of IpaD promotes the aggregation of the protein by formation of intermolecular hydrogen bonding. A more complex behavior with the temperature was observed for the three major bands. For example, the band at 1643 cm^{-1} displayed evidence for multiple transitions, with an overall increase in the area with temperature (Figure 4C). In good agreement with the CD experiments, IpaD$^{\Delta 1-120}$ only showed the transition at high temperatures, with no evidence of minor transitions as seen for the IpaD wild type (Figure 4C).

Analysis of the Tertiary Structure by Fluorescence Spectroscopy. Because IpaD possesses four tryptophan residues, fluorescence spectroscopy was used to monitor changes in the tertiary structure of IpaD. Intrinsic tryptophan fluorescence is highly environmentally sensitive and is widely used to monitor changes in tryptophan microenvironments result-

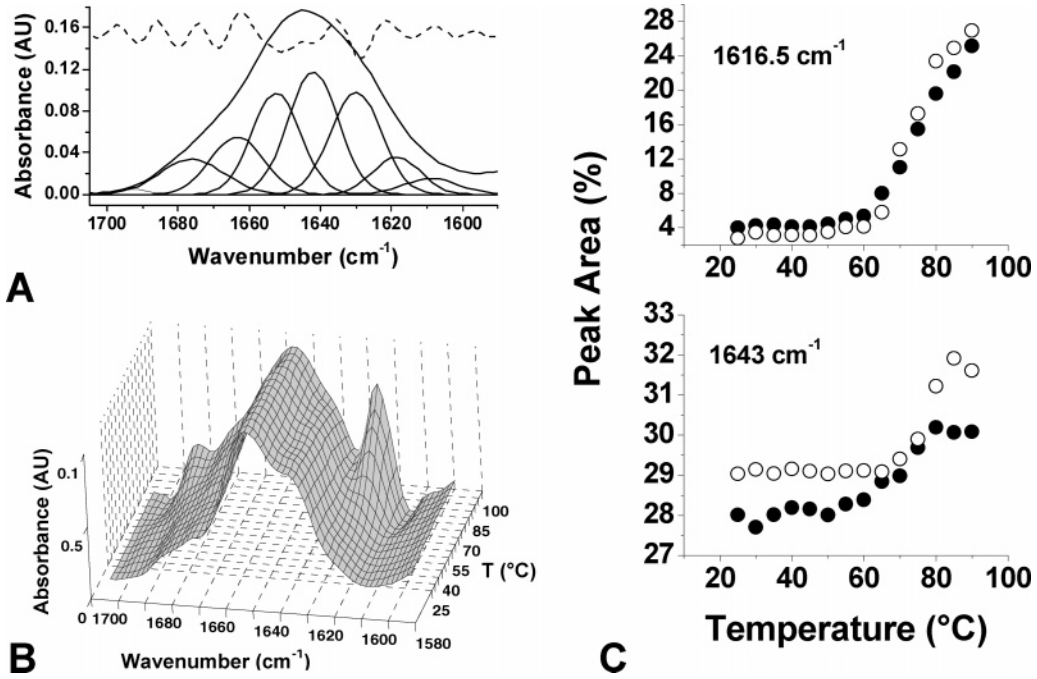

FIGURE 4: FTIR study of IpaD in D_2O. (A) Deconvoluted amide I′ of IpaD in solution measured by ATR−FTIR (15 mg/mL, pD = 7.0). The dotted line represents the second derivative trace of the amide I′, which was used for initial positioning of the individual Gaussian components. (B) Fourier self-deconvolution of the amide I′ of IpaD at different temperatures (bandwidth = 17 cm^{-1}; band-narrowing factor of 2.0). (C) Thermal behavior of the amide I′ bands at 1616.5 cm^{-1} (top) and 1643 cm^{-1} (bottom) for IpaD (●) and IpaD $^{\Delta 1-120}$ (○). Spectra presented are an average of 256 scans.

Table 2: Thermally Induced Unfolding of IpaD and IpaD Mutants Evaluated by Spectroscopic and Calorimetric Techniques

	CD[a]		Trp fluorescence[a]		ANS fluorescence[a]		DSC[b]	
protein	first midpoint	second midpoint	first midpoint	second midpoint	first midpoint	second midpoint	first midpoint	second midpoint
IpaD	59.5 (0.1[c])	79.6 (0.3)	56.5 (1.7)	73.8 (1.7)	51.5 (0.6)	75.8 (1.0)	59.6 (0.3)	77.2 (0.5)
IpaD$^{\Delta 41-80}$	ND[d]	79.6 (0.6)	ND	79.2 (1.4)	ND	77.2 (0.9)	59.3[e] (6.3)	76.9 (0.5)
IpaD$^{\Delta 81-120}$	ND	76.7 (0.4)	ND	78.8 (1.7)	ND	74.9 (0.9)	ND	76.1 (0.1)
IpaD$^{\Delta 1-120}$	ND	76.3 (0.7)	ND	77.5 (0)	ND	76.6 (0.6)	ND	73.6 (1.4)

[a] Midpoints determined by derivative analysis. [b] Midpoint determined by fitting the thermograms to a non-two-state unfolding model. [c] Standard error ($n = 3$). [d] ND = not detected. [e] When a minor transition was evident (see Figure 5), a precise midpoint of the transition could not be determined.

ing from alterations in the tertiary structure of proteins. Exposure to more polar environments generally results in the tryptophan emission being shifted to a longer wavelength (red shift), while the movement into more apolar environments results in a blue shift (*35*). The four tryptophan residues in IpaD are within the C-terminal domain, with two of the four lying within the predicted coiled coil and two present between the coils. The tryptophan emission spectrum of IpaD showed a maximum at 329 nm, indicating that the four tryptophans are on average buried within the apolar core of the IpaD structure. The emission maxima for the N-terminal mutants were red-shifted with respect to the spectrum of the wild-type protein (Figure 5A). The largest shift (~4 nm) was observed for the largest deletion mutant IpaD $^{\Delta 1-120}$. Because all four tryptophans are retained in these N-terminal IpaD mutants, it seems that deletion of the N-terminal domain causes an increased exposure of these residues to the aqueous environment, perhaps because of induced rearrangements in the tertiary structure of the C-terminal domain or the simple uncovering of regions that were less solvent-exposed in the full-length protein as a result of being hidden by the presumptive domain−domain interactions. On the basis of FTIR results showing that the dominant coiled-coil features of IpaD are retained in these deletion mutants, any induced rearrangements would seem to be of limited magnitude. These changes may also indicate some degree of domain−domain interaction. Changes in the tryptophan maximum emission wavelength of IpaD (Figure 5B) showed thermal transitions centered at about 57 °C (50−70 °C) and 75 °C (72−77 °C), which are similar to but slightly lower than those detected by CD analysis (Table 2). All three of the deletion mutants exhibited a single transition between 70 and 82 °C, which is consistent with the CD data (Figure 3 and Table 2). Because none of the tryptophans are located within the deleted region, it is possible that the unfolding of the N-terminal domain induces partial exposure of one or more of the tryptophan residues of the C-terminal domain in the same manner that deletion of the N-terminal domain does. Thus, both domains presumably expose apolar regions upon unfolding.

To further characterize changes in the tertiary structure of IpaD, the thermal unfolding of the proteins was evaluated in the presence of ANS, an extrinsic probe that often binds to apolar regions of proteins. The fluorescence of ANS is highly quenched in aqueous solution but can increase dramatically upon binding to protein apolar regions (*36*). When probed by ANS binding, IpaD showed two well-defined transitions at around 53 and 77 °C, which were

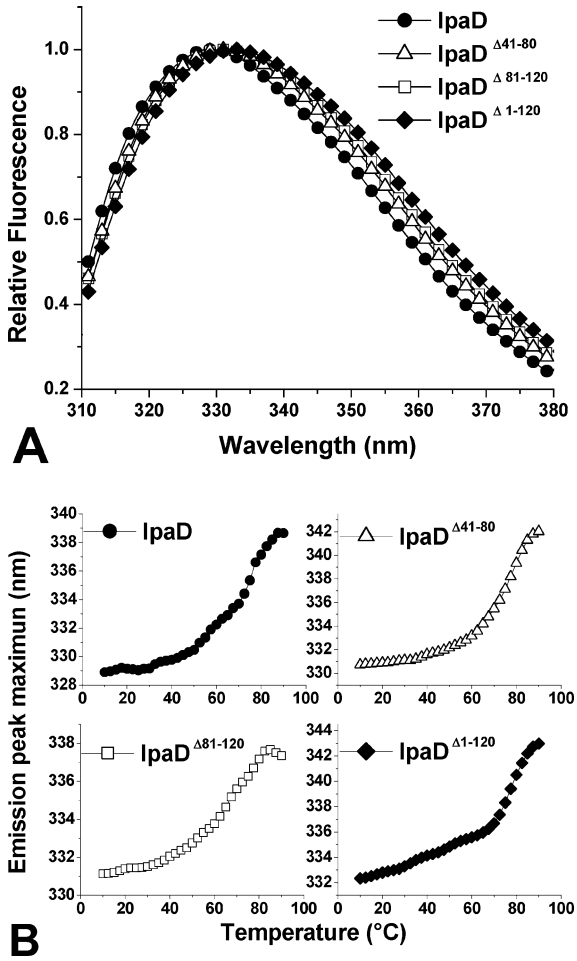

FIGURE 5: Analysis of the tertiary-structure stability of IpaD and mutants using intrinsic fluorescence spectroscopy. (A) Trp emission spectra of IpaD and N-terminal deletion mutants show elimination of regions of the N-terminal domain results in spectral red shifts for the four Trp residues located in the C-terminal domain. (B) Effect of the temperature on the wavelength of the Trp fluorescence emission of IpaD. Spectra were collected from 10 to 90 °C at 2.5 °C intervals with a 3 min equilibration time at each temperature. The protein concentration was 0.1 mg/mL in each experiment. Although the error bars have been omitted for clarity, the individual data entries have a typical uncertainty of 5% or less ($n = 3$).

attributable to the exposure of apolar regions because of the conformational alterations within the two individual domains (Figure 6). Again, a slight reduction in the T_m of the first transition is seen compared to both CD (3.5 °C) and intrinsic fluorescence (6.5 °C). All three N-terminal mutants showed only a small transition near 75−77 °C, confirming the CD spectroscopy observations (Figure 6).

Aggregation of IpaD and Mutants. The associative behavior of IpaD was evaluated by monitoring the turbidity (OD) at 360 nm as the temperature was increased (Figure 7). Full-length IpaD showed a large increase in turbidity starting at around 70 °C with a transition around 77 °C. The three N-terminal deletion mutants showed similar aggregation behavior with comparable transition temperatures (Figure 7). The drop in aggregation after the transition is due to the precipitation of aggregates within the cuvette. It is noteworthy that no aggregation was detected around 60 °C, the temperature that corresponds to the minor transition event. These results are in agreement with the FTIR observations that indicate that the unfolding of the major C-terminal domain is the major determinant for the aggregation of the protein.

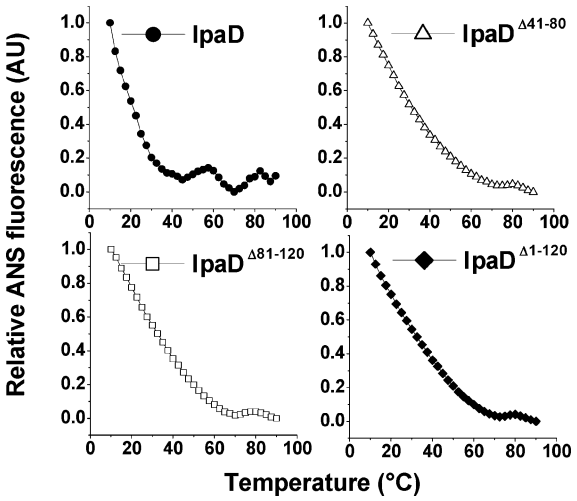

FIGURE 6: Binding of ANS to IpaD and deletion mutants. A solution containing IpaD and N-terminal deletion mutants (0.1 mg/mL) in the presence of 40 μM ANS was excited at 385 nm, and the fluorescence intensity at 485 nm was monitored as a function of the temperature. Although the error bars have been omitted for clarity, the individual data entries have a typical uncertainty of less than 5% ($n = 3$).

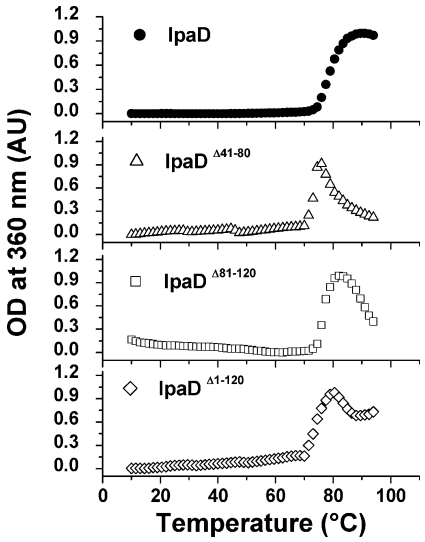

FIGURE 7: Temperature-induced aggregation of IpaD and deletion mutants. The turbidity of IpaD and mutants (0.1 mg/mL) was studied by monitoring the OD at 360 nm as a function of the temperature. Although the error bars have been omitted for clarity, the individual data entries have a typical uncertainty of less than 5% ($n = 3$).

Analysis of the Thermal Unfolding of IpaD and Mutants Measured by DSC. Calorimetry is another useful method for analyzing the thermal unfolding of proteins with the potential to provide a direct energetic description of distinct protein-unfolding events. The thermogram for IpaD shows two transitions, with a minor transition having a T_m around 59 °C and a main transition between 70 and 85 °C with a T_m near 77 °C (Figure 8 and Table 2). A non-two-state model was employed to analyze the DSC thermograms of IpaD and the deletion mutants to estimate the transition temperatures (Table 2) (*28*). A second heating run across the full temperature range (data not shown) revealed that the thermally induced changes were irreversible. As observed by CD spectroscopy, however, the first-transition event was found to be reversible, permitting thermodynamic analysis of this single event. Using a non-two-state model to analyze

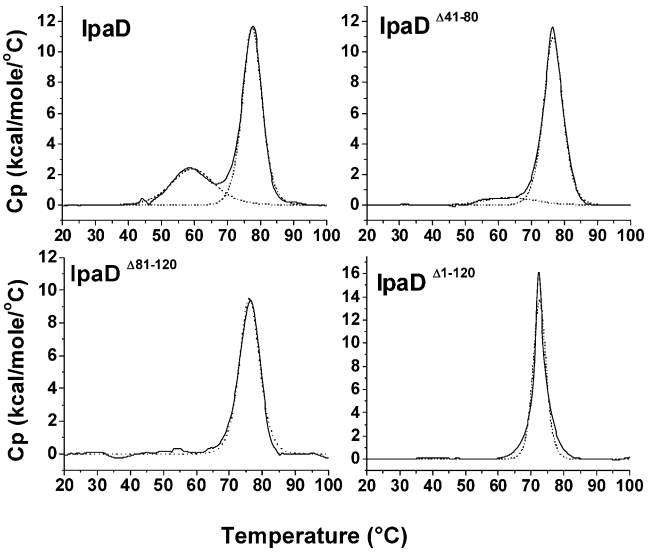

FIGURE 8: DSC thermograms of IpaD and deletion mutants. The dotted line is a theoretical fit using a non-two-state model. A protein concentration of 2 mg/mL was used.

this first transition, the standard free energy ($\Delta G°$) and the unfolding enthalpy change (ΔH^{T_m}) of this domain were found to be 0.86 and 18.4 kcal/mol, respectively.

The presence of two peaks for IpaD unfolding confirms the spectroscopic observations that at least two domains exist within IpaD. The DSC thermograms showed that all three N-terminal mutants exhibit major transitions with little or no minor transitions (Figure 8 and Table 2). IpaD$^{\Delta 41-80}$, however, does show a very slight early transition, but the magnitude was significantly lower than that of IpaD, with a very large standard deviation making precise definition of this endotherm difficult (Figure 8 and Table 2). Altogether, the results again indicate that the less stable domain of IpaD is located at its N terminus. It also appears that the two domains unfold independently because the absence of the N-terminal domain did not significantly affect the stability of the C-terminal region.

DISCUSSION

While many facets of *Shigella* virulence have been explored, an overlooked but essential contributor to the invasion of *Shigella* to human cells is IpaD, whose virulence role remains an enigma. A recent analysis of IpaD, however, revealed that it plays a central role in the *Shigella* invasion process after being located at the tip of the *Shigella* TTSS needle (Espina et al., *Infect. Immun.*, in press). Although tremendous strides are now being made in identifying the biological functions of IpaD, no structural information is yet available to provide any information concerning the structure/function relationship of this protein. Therefore, the focus of this study was to examine the solution behavior of recombinant IpaD and IpaD deletion mutants to search for correlations with newly identified biological activities.

IpaD is highly soluble in aqueous solution and possesses a substantial amount of α-helical structure. When thermal unfolding was examined as a measure of protein stability, IpaD demonstrated a two-stage unfolding process, suggesting the presence of independently folding domains with distinct thermal stabilities. This two-step unfolding, however, was not seen following the deletion of the N-terminal 120 residues, even though the remaining C-terminal portion of the protein continued to be soluble and retained a highly stable, α-helical character. These data imply that the N-terminal 120 amino acids (approximately) of IpaD form an independent structural domain that folds at least partially independently of a larger and more stable C-terminal domain. FTIR spectroscopy strongly suggests a significant intramolecular coiled coil within the C-terminal domain of IpaD and accounts for the high stability of this portion of the protein. Likewise, the presence of a coiled coil as the structural core of the C-terminal domain could explain why deletions within this part of the protein cause it to be partitioned into inclusion bodies in *E. coli* and cause it to be degraded in *S. flexneri*. When the intrinsic tryptophan fluorescence of IpaD was examined, deletion of IpaD residues 1−120 resulted in a detectable spectral red shift, despite the fact that all of the Trp residues are located in the C-terminal two-thirds of the protein. Because FTIR demonstrated that the C-terminal domain does not undergo major structural changes upon deletion of the N-terminal domain, this red shift suggests that the N-terminal domain is able to influence the C-terminal Trp residues either because of their presence at the interface between the two domains or because of subtle structural changes in the more stable C-terminal domain caused by the absence of the N-terminal region. Binding of ANS as a function of the temperature also suggests the existence of two structural domains for IpaD. CD and aggregation data indicated that the less stable N-terminal domain could be successfully refolded and that its unfolded state does not give rise to the aggregation of IpaD. Aggregation does occur, however, upon unfolding of the C-terminal domain, whose unfolding is not reversible.

The biophysical data strongly suggest that IpaD contains two independent domains, with the N-terminal 120 amino acids forming a relatively thermal labile structure and the C-terminal domain (120−332) comprising a second highly stable independently folded unit. Much of the existing functional data on IpaD can be interpreted by this two-domain model. Deletions within the IpaD N-terminal domain do not affect the global stability of the protein in vivo and do not completely abrogate the ability for strains expressing the mutant proteins to invade cells or to properly localize IpaD to the needle tip. These same deletions, however, greatly compromise the productive secretion and insertion of IpaB and IpaC into host-cell membranes, a step that defines the transition from quiescent to invasive *S. flexneri.* Thus, it could be speculated that the structural properties that cause the N-terminal domain to fold independently may be integral for interdomain communication with the structurally stable core of the C-terminal domain. Globally, this domain−domain communication that occurs upon host-cell contact may be responsible for triggering the secretion and, more importantly, proper presentation of IpaB and IpaC to the host cell.

Mutations within the IpaD C-terminal domain abolish secretion control, invasion, contact hemolysis, and localization of the IpaD to the needle tip (Espina et al., *Infect. Immun.*, in press). Biophysical data indicate that this domain is highly stable, containing a coiled coil. Thus, the mutations made within the C-terminal domain would be expected to destroy the structural integrity of the coiled coil and, thus, the entire region, preventing the formation of a functional

protein. Because even small mutations at the very C terminus of this domain abolish needle-tip localization, this domain must be responsible for the interactions involved in maintaining IpaD at the needle tip. Tip interaction appears to be required to prevent the massive uninduced release of effectors through the TTSS needle (Espina et al., *Infect. Immun.*, in press). Therefore, in contrast to the thermally labile N-terminal domain, the highly stable C-terminal domain probably gives rise to the core structure of the protein, which is needed to maintain the protein in its proper position atop the *Shigella* TTSS needle.

Although there is little sequence homology between IpaD and LcrV of *Yersinia* spp., they both are needed for the presentation of translocator pore proteins to target cell membranes (*11*, *16*). LcrV has been shown to form a unique complex at the *Yersinia* TTSS needle tip. Additionally, it was demonstrated that the LcrV orthologues PcrV and AcrV of *Pseudomonas* and *Aeromonas*, respectively, could complement a *lcrV* null mutant and form a similar tip complex (*14*). The crystal structure of LcrV has been solved, revealing an N-terminal domain hinged to a C-terminal domain consisting of a long coiled coil (*18*) that is consistent with the structure proposed here for IpaD. Because PcrV and AcrV can functionally complement LcrV, it is assumed that their atomic structures will be conserved. The greatest divergence between these three proteins is at the N terminus. Not only are the sequences of the N-terminal domains variable, but relative to LcrV, this domain is smaller in PcrV and larger in AcrV. It is noteworthy that the tip complexes formed by these three proteins can be distinguished by their sizes at the base of the complex next to the needle, which, relative to LcrV, is smaller for PcrV and larger for AcrV. Whether this reflects the structure of a discrete N-terminal domain has yet to be determined. Furthermore, whether this is the actual location of the N-terminal domain of IpaD is speculative. Undoubtedly, the recent solution of the structures of the TTSS needle proteins of *Burkholderia pseudomallei* and *S. flexneri* will shed light on the structure of the TTSS needle and the possible positioning of the tip protein complex atop the needle (*37*) (Deane et al., manuscript submitted).

The data presented here are consistent with IpaD being a two-domain protein that plays a central role in the virulence of *S. flexneri*. They also argue that similar studies would be useful in exploring the structure−function relationships of IpaD homologues from other bacterial pathogens, such as SipD from *Salmonella* (*38*), and BipD from *Burkholderia* (*39*), or perhaps even more distantly related homologues, such as LcrV from *Yersinia* (*40*) and PcrV from *Pseudomonas* (*17*). A combination of biological/functional characterization of these proteins in light of their biophysical properties and, eventually, high-resolution structures will provide significant insight into their mechanistic roles in bacterial pathogenesis. Such information will be valuable for developing new approaches to disease prevention and treatment.

ACKNOWLEDGMENT

Technical assistance from Numukunda Darboe, Roma Kenjale, and Lingling Zhang is gratefully acknowledged. Critical reading of the manuscript by members of the Picking lab is also acknowledged.

REFERENCES

1. Cossart, P., and Sansonetti, P. J. (2004) Bacterial invasion: The paradigms of enteroinvasive pathogens, *Science 304*, 242−248.
2. Sasakawa, C., Kamata, K., Sakai, T., Makino, S., Yamada, M., Okada, N., and Yoshikawa, M. (1988) Virulence-associated genetic regions comprising 31 kilobases of the 230-kilobase plasmid in *Shigella flexneri* 2a, *J. Bacteriol. 170*, 2480−2484.
3. Menard, R., Sansonetti, P., Parsot, C., and Vasselon, T. (1994) Extracellular association and cytoplasmic partitioning of the IpaB and IpaC invasins of *S. flexneri*, *Cell 79*, 515−525.
4. Tran Van Nhieu, G., Bourdet-Sicard, R., Dumenil, G., Blocker, A., and Sansonetti, P. J. (2000) Bacterial signals and cell responses during *Shigella* entry into epithelial cells, *Cell Microbiol. 2*, 187−193.
5. Menard, R., Sansonetti, P. J., and Parsot, C. (1993) Nonpolar mutagenesis of the ipa genes defines IpaB, IpaC, and IpaD as effectors of *Shigella flexneri* entry into epithelial cells, *J. Bacteriol. 175*, 5899−5906.
6. Menard, R., Sansonetti, P., and Parsot, C. (1994) The secretion of the *Shigella flexneri* Ipa invasins is activated by epithelial cells and controlled by IpaB and IpaD, *EMBO J. 13*, 5293−5302.
7. Blocker, A., Gounon, P., Larquet, E., Niebuhr, K., Cabiaux, V., Parsot, C., and Sansonetti, P. (1999) The tripartite type III secreton of *Shigella flexneri* inserts IpaB and IpaC into host membranes, *J. Cell Biol. 147*, 683−693.
8. Tran, N., Serfis, A. B., Osiecki, J. C., Picking, W. L., Coye, L., Davis, R., and Picking, W. D. (2000) Interaction of *Shigella flexneri* IpaC with model membranes correlates with effects on cultured cells, *Infect. Immun. 68*, 3710−3715.
9. Tran Van Nhieu, G., Caron, E., Hall, A., and Sansonetti, P. J. (1999) IpaC induces actin polymerization and filopodia formation during *Shigella* entry into epithelial cells, *EMBO J. 18*, 3249−3262.
10. Zychlinsky, A., Kenny, B., Menard, R., Prevost, M. C., Holland, I. B., and Sansonetti, P. J. (1994) IpaB mediates macrophage apoptosis induced by *Shigella flexneri*, *Mol. Microbiol. 11*, 619−627.
11. Picking, W. L., Nishioka, H., Hearn, P. D., Baxter, M. A., Harrington, A. T., Blocker, A., and Picking, W. D. (2005) IpaD of *Shigella* is independently required for regulation of Ipa protein secretion and efficient insertion of IpaB and IpaC into host membranes, *Infect. Immun. 73*, 1432−1440.
12. Harrington, A. T., Hearn, P. D., Picking, W. L., Barker, J. R., Wessel, A., and Picking, W. D. (2003) Structural characterization of the N terminus of IpaC from *Shigella flexneri*, *Infect. Immun. 71*, 1255−1264.
13. Lloyd, S. A., Sjostrom, M., Andersson, S., and Wolf-Watz, H. (2002) Molecular characterization of type III secretion signals via analysis of synthetic N-terminal amino acid sequences, *Mol. Microbiol. 43*, 51−59.
14. Mueller, C. A., Broz, P., Muller, S. A., Ringler, P., Erne-Brand, F., Sorg, I., Kuhn, M., Engel, A., and Cornelis, G. R. (2005) The V-antigen of *Yersinia* forms a distinct structure at the tip of injectisome needles, *Science 310*, 674−676.
15. Fields, K. A., Nilles, M. L., Cowan, C., and Straley, S. C. (1999) Virulence role of V antigen of *Yersinia pestis* at the bacterial surface, *Infect. Immun. 67*, 5395−5408.
16. Marenne, M. N., Journet, L., Mota, L. J., and Cornelis, G. R. (2003) Genetic analysis of the formation of the Ysc−Yop translocation pore in macrophages by *Yersinia enterocolitica*: Role of LcrV, YscF and YopN, *Microb. Pathog. 35*, 243−258.
17. Goure, J., Broz, P., Attree, O., Cornelis, G. R., and Attree, I. (2005) Protective anti-V antibodies inhibit *Pseudomonas* and *Yersinia* translocon assembly within host membranes, *J. Infect. Dis. 192*, 218−225.
18. Derewenda, U., Mateja, A., Devedjiev, Y., Routzahn, K. M., Evdokimov, A. G., Derewenda, Z. S., and Waugh, D. S. (2004) The structure of *Yersinia pestis* V-antigen, an essential virulence factor and mediator of immunity against plague, *Structure 12*, 301−306.
19. Marquart, M. E., Picking, W. L., and Picking, W. D. (1995) Structural analysis of invasion plasmid antigen D (IpaD) from *Shigella flexneri*, *Biochem. Biophys. Res. Commun. 214*, 963−970.
20. Mach, H., Middaugh, C. R., and Lewis, R. V. (1992) Statistical determination of the average values of the extinction coefficients of tryptophan and tyrosine in native proteins, *Anal. Biochem. 200*, 74−80.

21. Edelhoch, H. (1967) Spectroscopic determination of tryptophan and tyrosine in proteins, *Biochemistry 6*, 1948−1954.
22. Lobley, A., Whitmore, L., and Wallace, B. A. (2002) DICHROWEB: An interactive website for the analysis of protein secondary structure from circular dichroism spectra, *Bioinformatics 18*, 211−212.
23. Whitmore, L., and Wallace, B. A. (2004) DICHROWEB: An online server for protein secondary structure analyses from circular dichroism spectroscopic data, *Nucleic Acids Res. 32*, W668−W673.
24. Sreerema, N. W., and Woody, R. W. (1990) A self-consistent method for the analysis of protein secondary structure from circular dichroism, *Anal. Biochem. 209*, 32−44.
25. Provencher, S. W., and Glockner, J. (1981) Estimation of globular protein secondary structure from circular dichroism, *Biochemistry 20*, 33−37.
26. Manavalan, P., and Johnson, W. C., Jr. (1987) Variable selection method improves the prediction of protein secondary structure from circular dichroism spectra, *Anal. Biochem. 167*, 76−85.
27. Kueltzo, L. A., Osiecki, J., Barker, J., Picking, W. L., Ersoy, B., Picking, W. D., and Middaugh, C. R. (2003) Structure−function analysis of invasion plasmid antigen C (IpaC) from *Shigella flexneri*, *J. Biol. Chem. 278*, 2792−2798.
28. Sanchez-Ruiz, J. M. (1992) Theoretical analysis of Lumry−Eyring models in differential scanning calorimetry, *Biophys. J. 61*, 921−935.
29. Susi, H., and Byler, D. M. (1986) Resolution-enhanced Fourier transform infrared spectroscopy of enzymes, *Methods Enzymol. 130*, 290−311.
30. Heimburg, T., Schuenemann, J., Weber, K., and Geisler, N. (1996) Specific recognition of coiled coils by infrared spectroscopy: Analysis of the three structural domains of type III intermediate filament proteins, *Biochemistry 35*, 1375−1382.
31. Heimburg, T., Schunemann, J., Weber, K., and Geisler, N. (1999) FTIR spectroscopy of multistranded coiled coil proteins, *Biochemistry 38*, 12727−12734.
32. Lupas, A., Van Dyke, M., and Stock, J. (1991) Predicting coiled coils from protein sequences, *Science 252*, 1162−1164.
33. Arrondo, J. L., Castresana, J., Valpuesta, J. M., and Goni, F. M. (1994) Structure and thermal denaturation of crystalline and noncrystalline cytochrome oxidase as studied by infrared spectroscopy, *Biochemistry 33*, 11650−11655.
34. Murayama, K., and Tomida, M. (2004) Heat-induced secondary structure and conformation change of bovine serum albumin investigated by Fourier transform infrared spectroscopy, *Biochemistry 43*, 11526−11532.
35. Lakowicz, J. R. (1983) *Principles of Fluorescence Spectroscopy*, Plenum Press, New York.
36. Rosen, C. G., and Weber, G. (1969) Dimer formation from 1-amino-8-naphthalenesulfonate catalyzed by bovine serum albumin. A new fluorescent molecule with exceptional binding properties, *Biochemistry 8*, 3915−3920.
37. Zhang, L., Wang, Y., Picking, W. L., Picking, W. D., and DeGuzman, R. N. (2006) Solution structure of monomeric BsaL, the type III secretion needle protein of *Burkholderia pseudomallei*, *J. Mol. Biol.*, in press.
38. Kaniga, K., Trollinger, D., and Galan, J. E. (1995) Identification of two targets of the type III protein secretion system encoded by the *inv* and *spa* loci of *Salmonella typhimurium* that have homology to the *Shigella* IpaD and IpaA proteins, *J. Bacteriol. 177*, 7078−7085.
39. Stevens, M. P., Haque, A., Atkins, T., Hill, J., Wood, M. W., Easton, A., Nelson, M., Underwood-Fowler, C., Titball, R. W., Bancroft, G. J., and Galyov, E. E. (2004) Attenuated virulence and protective efficacy of a *Burkholderia pseudomallei bsa* type III secretion mutant in murine models of melioidosis, *Microbiology 150*, 2669−2676.
40. Une, T., and Brubaker, R. R. (1984) Roles of V antigen in promoting virulence and immunity in yersiniae, *J. Immunol. 133*, 2226−2230.

BI060625V